Research Square

Preprints are preliminary reports that have not undergone peer review.
They should not be considered conclusive, used to inform clinical practice,
or referenced by the media as validated information.

A Novel Approach to Computing the Permanent Magnet Thickness in PMSMs

Duan weichuan
Bohai University
Li Ming
liming1@qymail.bhu.edu.cn

Bohai University
Lun Shuxian
Bohai University

Research Article

Keywords: PMSM, PM thickness, leakage coefficient, reluctivity, iterative calculation, FE analysis

Posted Date: September 7th, 2026

DOI: https://doi.org/10.21203/rs.3.rs-10429940/v1

License: This work is licensed under a Creative Commons Attribution 4.0 International License.
Read Full License

Additional Declarations: No competing interests reported.

A Novel Approach to Computing the Permanent Magnet Thickness in PMSMs

Duan weichuan[1] · Li Ming[1] · Lun shuxian[1]

Abstract
To address the low accuracy of empirical formulas and the time-consuming nature of finite-element (FE) parametric sweeps for permanent magnet (PM) thickness in permanent magnet synchronous motors (PMSMs), a novel iterative approach for calculating the PM thickness is presented. The method first establishes a FE model using an initial thickness, extracts the leakage factor, reluctivity, and average air-gap flux density, and then iteratively updates the thickness using the calculation formula. A 1600 kW, 250 r/min U-shaped interior PMSM is taken as the test case for validation. The results indicate that the proposed method reduces the calculation time by about 75% compared to the FE parametric sweep method, and yields identical thickness results. Both electromagnetic performance analysis and prototype tests confirm that the proposed method enhances design efficiency without sacrificing accuracy, and is applicable to the fast calculation of PM thickness for PMSMs.
Keywords PMSM· PM thickness· leakage coefficient· reluctivity· iterative calculation· FE analysis.

1 Introduction

In recent years, permanent magnet synchronous motors (PMSMs) have been widely used in mining equipment, marine propulsion, wind power generation, and electric drives [1-4]. In PMSMs, the permanent magnet (PM) thickness is a key structural parameter that affects both motor performance and manufacturing cost. Therefore, quickly and accurately calculating the PM thickness while meeting electromagnetic performance requirements is of great significance for shortening the design cycle, reducing PM consumption, and improving motor design efficiency.

At present, the calculation methods for PM thickness mainly include the empirical formula method and the finite element (FE) parametric sweep method. The empirical formula method calculates the PM thickness based on the equivalent magnetic circuit theory. In [5], an analytical method for calculating the air-gap flux of interior PMSMs developed; by depicting the relationships among PM flux, leakage flux, and air-gap flux via an analytical model, it offers a fast calculation concept for the initial design of PMSMs. The aforementioned studies indicate that the empirical formula method features fast computation speed and requires few parameters, making it suitable for the initial design stage of electric motors [6]. However, the parameters in this method, such as the leakage coefficient, reluctivity, and structural correction factor, usually rely on empirical values, which can easily lead to PM thickness calculation errors when the motor structure is complex or when significant local magnetic saturation occurs.

The FE parametric sweep method determines a preferable PM thickness by building FE models under different PM thicknesses and comparatively analyzing the air-gap flux density, back-EMF, torque, and losses. In [7], an axial-flux PMSM featuring non-uniform-thickness magnets was studied; using the PM thickness and pole-arc coefficient as optimization variables, the effects of various structural parameters on electromagnetic performance were examined, showing that the FE method is capable of faithfully capturing the influence of PM structure changes on motor behavior. In [8], the structural optimization of a PMSM was accomplished via parametric modeling and repeated FE analyses, indicating that the FE sweep parametric method is well suited for performance validation and structural refinement of motors. The FE parametric sweep method can reasonably account for motor geometry, material nonlinearity, local saturation, and leakage flux effects; however, it requires repeated modeling, solving, and post-processing for multiple design candidates, leading to a long computation cycle and significantly increased computation time and design cost [9-10].

To address the problems of insufficient accuracy in the empirical formula method and the long computation cycle of the FE parametric sweep method, this paper proposes a PM thickness calculation method based on the iteration of the leakage coefficient, reluctivity, and average air-gap flux density. This method first builds a corresponding FE model using an initial value of the PM thickness, then extracts the main air-gap flux, total PM flux, and magnetic potential differences across various parts through FE post-processing to update the key parameters; finally, the updated parameters are substituted back into the PM thickness calculation formula, and the relative error between the thickness results of two consecutive iterations is used as the convergence criterion, thereby rapidly determining the PM thickness. This paper takes a 1600 kW, 250 r/min low-speed high-torque U-shaped interior PMSM as the research object to verify the proposed method. The main structure of this paper is arranged as follows: Section 2 introduces the iterative PM thickness calculation method proposed in this paper, including the definitions of key parameters, the derivation of the PM thickness calculation formula, and the calculation flow. Section 3 takes the 1600 kW, 250 r/min U-shaped interior PMSM as an example, presents the iterative PM thickness results, and compares them with those obtained from the conventional empirical formula method and the FE parametric sweep method. Section 4 analyzes the no-load performance, load torque characteristics, and overall performance under different thickness schemes. Section 5 verifies the accuracy of the FE model through

prototype tests. Section 6 provides the conclusions of this paper.

2 PM Thickness Calculation Method

2.1 Empirical Formula Method

In the preliminary design of PMSMs, the PM thickness can usually be estimated using an empirical formula based on the equivalent magnetic circuit method. This method models the main magnetic circuit of the motor as an equivalent magnetic circuit consisting of the PMs, air gap, stator and rotor cores, and leakage flux branches, and derives the PM thickness calculation formula by establishing the relationship between the magnetomotive force of the PMs and that of the external magnetic circuit. The empirical formula for calculating the PM thickness can be expressed as [11]:

$$h_m = \frac{\mu_r K_R K_a b_m \delta_e}{\sigma_0 (1 - b_m)} \tag{1}$$

where h_m is the PM thickness; μ_r is the relative recoil permeability of the PM; K_R is the reluctivity; K_a is the structural correction factor; b_m is the PM operating point coefficient; σ_0 is the leakage coefficient; and δ_e is the air-gap length.

As can be seen from (1), the empirical formula introduces the effects of leakage flux, core magnetic potential difference, and structural influences into the PM thickness calculation through parameters such as the leakage coefficient, reluctivity, and structural correction factor. This method features a simple calculation process, can quickly obtain the initial value of the PM thickness, and is suitable for the preliminary design stage of motors. However, some parameters in the formula usually rely on empirical values. When the motor structure, magnetic circuit saturation level, or leakage flux distribution changes, fixed empirical parameters cannot accurately reflect the actual magnetic circuit state, which easily leads to PM thickness calculation errors. Therefore, although the traditional empirical formula method has the advantage of fast computation speed, it still needs to be combined with more accurate magnetic field analysis results to correct the key parameters.

2.2 A Novel Computational Method

The PM thickness calculation method proposed in this paper is an improvement upon the conventional equivalent magnetic circuit method. Unlike the traditional empirical formula method, this paper no longer treats the leakage coefficient and reluctivity as fixed empirical parameters; instead, they are regarded as calculation parameters that vary with the PM thickness and magnetic circuit state, and are updated using FE post-processing results. More specifically, the calculation of PM thickness in this method primarily involves the leakage factor, reluctivity, average air-gap flux density, remanent flux density of the PM, pole-arc factor, and air-gap length. Among these, the leakage coefficient is determined by the ratio of the total PM flux to the main air-gap flux, reflecting the extent to which the PM flux enters the main magnetic circuit of the air gap; the PM is determined by the ratio of the total magnetic potential difference of the external magnetic circuit to the air-gap magnetic potential difference, reflecting the influence of the core magnetic potential difference and local saturation on the magnetomotive force requirement of the PM; and the average air-gap flux density characterizes the magnetic loading level of the motor.

(1). Leakage Coefficient

The total flux generated by the PMs does not entirely enter the main air-gap magnetic circuit, but is divided into the main air-gap flux and leakage flux, which can be expressed as:

$$\Phi_M = \Phi_\delta + \Phi_\sigma \tag{2}$$

where Φ_M is the total PM flux, Φ_δ is the main flux entering the air gap, and Φ_σ is the leakage flux of the PM. To describe the utilization of the PM flux, the leakage coefficient is introduced, which is defined as the ratio of the total PM flux to the main air-gap flux [12]:

$$\sigma = \frac{\Phi_M}{\Phi_\delta} = 1 + \frac{\Phi_\sigma}{\Phi_\delta} \tag{3}$$

It can be seen from (3) that a larger leakage coefficient indicates more leakage flux that does not enter the main air-gap magnetic circuit, resulting in a lower utilization rate of the PM flux. In the traditional empirical formula, the leakage coefficient is usually taken as an empirical value. In this paper, the total PM flux and the main air-gap flux are respectively extracted through FE post-processing, and the leakage coefficient is iteratively updated so that it can reflect the leakage flux condition under the actual motor structure.

(2). Reluctivity

In a PMSM, the magnetomotive force provided by the PMs must overcome not only the air-gap magnetic potential difference but also the magnetic potential differences in the stator teeth, stator yoke, rotor yoke, and magnetic bridge regions; therefore, the air-gap magnetic potential difference is:

$$F_\delta = \frac{B_\delta}{\mu_0} \delta_e \tag{4}$$

where F_δ is the air-gap magnetic potential difference, B_δ is the air-gap flux density, δ_e is the air-gap length, and μ_0 is the permeability of vacuum. In addition to the air-gap magnetic potential difference, the external magnetic circuit also includes the magnetic potential difference in the stator teeth, stator yoke, rotor yoke, and the rotor magnetic bridges or locally saturated regions. Therefore, the total magnetic potential difference of the external magnetic circuit can be expressed as:

$$F_{ext} = F_\delta + F_{ts} + F_{ys} + F_{yr} + F_b \tag{5}$$

where F_{ts} is the magnetic potential difference of the stator teeth, F_{ys} is the magnetic potential difference of the stator yoke, F_{yr} is the magnetic potential difference of the rotor yoke, and F_b is the magnetic potential difference of

the magnetic bridge region. Therefore, the reluctivity can be expressed as [13]:

$$K_R = \frac{F_{\text{ext}}}{F_\delta} = 1 + \frac{F_t + F_{ys} + F_{yr} + F_b}{F_\delta} \tag{6}$$

It can be seen from (6) that when the saturation level of the core magnetic circuit increases, the magnetic potential differences in the stator teeth, yoke, and magnetic bridge regions increase, and the reluctivity also increases accordingly. In traditional empirical formulas, empirical values are usually adopted, making it difficult to reflect the changes in magnetic potential difference under different structures and magnetic loadings. This paper extracts the magnetic potential differences in the air gap and various iron core regions through FE post-processing, and updates them accordingly to make the PM thickness calculation closer to the actual magnetic circuit state.

(3). Average Air-Gap Flux Density

The average air-gap flux density is usually expressed as the main magnetic field level in the air gap of the motor. For PMSMs, the average air-gap flux density directly affects performance indicators such as the no-load back electromotive force, PM flux linkage, output torque, and power density. Therefore, in the calculation of PM thickness, the average air-gap flux density is an important calculation parameter and cannot be simply treated as a fixed empirical value. where the main air-gap flux per pole can be expressed as [14]:

$$\Phi_\delta = B_{avg} A_\delta \tag{7}$$

where B_{avg} is the average air-gap flux density, and A_δ is the equivalent air-gap area per pole. If the end effects are neglected, the equivalent air-gap area per pole can be approximately expressed as [14]:

$$A_\delta = \tau L_{ef} \tag{8}$$

where τ is the pole pitch, and L_{ef} is the effective core length. Therefore, the average air-gap flux density can be expressed as:

$$B_{avg} = \frac{\Phi_\delta}{A_\delta} = \frac{\Phi_\delta}{\tau L_{ef}} \tag{9}$$

As can be seen from (9), the average air-gap flux density is jointly determined by the main air-gap flux and the equivalent air-gap area per pole. In this paper, the main air-gap flux per pole is extracted through FE post-processing, and the average air-gap flux density is calculated in combination with the motor geometry, thereby enabling the average air-gap flux density to be updated with changes in the PM thickness and magnetic circuit state.

(4) Novel Formula for Calculating PM Thickness

Based on the parameter definitions presented above, the formula for calculating the PM thickness is derived in this section. For the main magnetic circuit under no-load condition, the flux generated by the PMs enters the main air-gap magnetic circuit after being affected by leakage flux, while the PM magnetomotive force is used to overcome the magnetic potential differences in the air gap and various parts of the external magnetic circuit. Since the definitions of the leakage coefficient, reluctivity, and average air-gap flux density have been given previously, this section directly performs the simultaneous derivation of the formula on this basis. From the definition of the leakage coefficient, it is known that the total PM flux and the main air-gap flux satisfy:

$$\Phi_M = \sigma \Phi_\delta \tag{10}$$

The total PM flux and the main air-gap flux are respectively expressed as:

$$\begin{aligned} \Phi_M &= B_m A_m \\ \Phi_\delta &= B_{\text{avg}} A_\delta \end{aligned} \tag{11}$$

where B_m is the flux density at the PM operating point, A_m is the effective area of the PM per pole, and A_δ is the equivalent air-gap area per pole. Using the pole-arc coefficient α_p to represent the relationship between the effective area of the PM and the equivalent air-gap area per pole, obtain:

$$A_m = \alpha_p A_\delta \tag{12}$$

Substituting the above formulas into the flux balance relationship, we obtain:

$$B_m \alpha_p A_\delta = \sigma B_{avg} A_\delta \tag{13}$$

The demagnetization curve of the PM near the operating point can be approximated as a linear relationship:

$$B_m = B_r + \mu_0 \mu_r H_m \tag{14}$$

where B_r is the remanence of the PM, μ_0 is the permeability of vacuum, μ_r is the relative recoil permeability of the PM, and H_m is the internal magnetic field intensity of the PM. Since the PM operates in the second quadrant of the demagnetization region, where $H_m < 0$, it follows that:

$$-H_m = \frac{B_r - B_m}{\mu_0 \mu_r} \tag{15}$$

From (12)-(15), we can derive:

$$-H_m = \frac{B_r - \dfrac{\sigma B_{avg}}{\alpha_p}}{\mu_0 \mu_r} \tag{16}$$

According to the equivalent magnetic circuit method, the magnetomotive force provided by the PMs should balance the magnetomotive force of the external magnetic circuit:

$$F_{ext} = K_R F_\delta \tag{17}$$

According to the definition of the reluctance coefficient, the total magnetic potential difference of the external magnetic circuit and the air-gap magnetic potential difference can be expressed as:

$$F_\delta = \frac{B_{avg}\delta_e}{\mu_0}$$
$$F_{ext} = K_R \frac{B_{avg}\delta_e}{\mu_0} \tag{18}$$

Substituting the PM demagnetization curve relationship and the external magnetic circuit magnetic potential difference relationship into the magnetomotive force balance equation, we obtain:

$$\frac{B_r - \frac{\sigma B_{avg}}{\alpha p}}{\mu_0 \mu_r} h_m = K_R \frac{B_{avg}\delta_e}{\mu_0} \tag{19}$$

From (19), the following can be derived after rearrangement:

$$h_m = \frac{\alpha_p \mu_r K_R B_{avg}\delta_e}{\alpha_p B_r - \sigma B_{avg}} \tag{20}$$

From (20), it can be seen that the PM thickness increases with the increase of the reluctance coefficient, average air-gap flux density, and air-gap length; meanwhile, an increase in the leakage coefficient reduces the effective denominator, thereby increasing the required PM thickness. To reduce the errors caused by fixed empirical parameters, this paper treats K_R, σ, and B_{avg} as iterative parameters that vary with the PM thickness. After the i-th FE calculation, $K_R^{(i)}$, $\sigma^{(i)}$, and $B_{avg}^{(i)}$ are obtained and then substituted into the thickness calculation formula to obtain the PM thickness for the next iteration:

$$h_m^{(i+1)} = \frac{\alpha_p \mu_r K_R^{(i)} B_{avg}^{(i)}\delta_e}{\alpha_p B_r - \sigma^{(i)} B_{avg}^{(i)}} \tag{21}$$

Therefore, the relative error between the thickness results of two consecutive iterations is defined as:

$$\varepsilon = \left| \frac{h_m^{(i+1)} - h_m^{(i)}}{h_m^{(i)}} \right| \times 100\%, \varepsilon < \varepsilon_0 \tag{22}$$

When the condition is satisfied, the calculation result is considered converged, and $h_m^{(i+1)}$ is taken as the final PM thickness. If the convergence condition is not satisfied, the PM thickness is updated with $h_m^{(i+1)}$, and the FE calculation and parameter extraction are repeated until the convergence requirement is met. At the same time, for the formula to be physically meaningful, it must hold that:

$$\alpha_p B_r - \sigma B_{avg} > 0 \tag{23}$$

If this term is less than or close to zero, it indicates that the average air-gap flux density is too high under the current conditions of PM remanence, leakage coefficient, and pole-arc coefficient, and the PM operating point is no longer reasonable; therefore, the values of B_{avg}, σ, α_p, or B_r need to be re-examined.

2.3 Calculation Flow of the Proposed PM Thickness

The iterative calculation flow for the PM thickness proposed in this paper is shown in Fig. 1. Based on the PM thickness calculation formula established above, this flow achieves rapid calculation of the PM thickness by continuously updating the leakage coefficient, reluctivity, and average air-gap flux density.

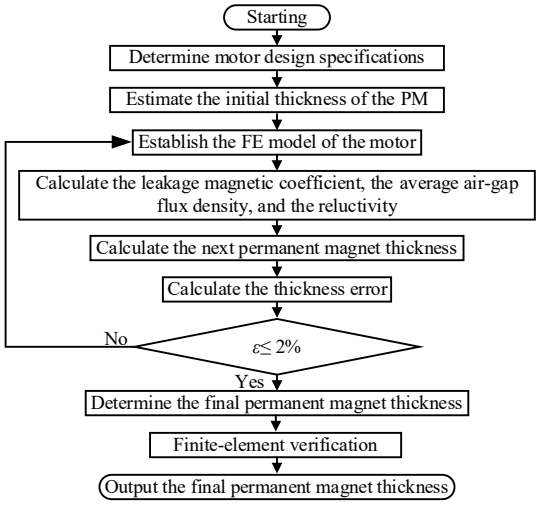


Fig.1. Flowchart of PM thickness calculation

As shown in Fig. 1, the calculation flow in this paper first inputs the basic design parameters of the motor and the parameters of the PM material. On this basis, an initial PM thickness $h_m^{(0)}$ is obtained. This initial thickness serves as the starting point for FE modeling. Subsequently, a FE model is established according to the current PM thickness $h_m^{(i)}$, no-load magnetic field calculations are carried out, parameters such as the total PM flux, main air-gap flux, air-gap magnetic potential difference, and total external-circuit magnetic potential difference are extracted, and the leakage coefficient, reluctivity, and average air-gap flux density for the current iteration are calculated accordingly. These are then substituted into the PM thickness calculation formula proposed in this paper to obtain the thickness for the next iteration, $h_m^{(i+1)}$. Since changes in the PM thickness further affect the air-gap flux density, leakage flux distribution, and local saturation levels, a convergence check must be performed on the results of two consecutive calculations. When the relative error between $h_m^{(i+1)}$ and $h_m^{(i)}$ is less than a preset threshold, the calculation is considered to have converged, and $h_m^{(i+1)}$ is taken as the final PM thickness; if the error does not meet the requirement, the model parameters are updated with $h_m^{(i+1)}$, and the FE calculation and parameter extraction are repeated until the convergence condition is satisfied. Through the above process, the proposed method uses FE analysis for the correction of key parameters, rather than directly conducting a large-scale thickness sweep. Therefore, this method not only retains the fast calculation speed characteristic of the empirical formula but also utilizes the FE results to correct errors caused by leakage flux, magnetic saturation, and changes in the magnetic circuit structure, providing a feasible calculation path for the rapid determination of the PM thickness.

3 Example Motor and Calculated Results

3.1 Parameters of the Example Motor

To verify the effectiveness of the iterative PM thickness calculation method proposed in this paper, a low-speed high-torque PMSM with a rated power of 1600 kW and a rated speed of 250 r/min is selected as the case-study object. This motor features a high-power rating, low speed, and large output torque, and imposes high requirements on the air-gap flux density, PM usage, and torque density; changes in the PM thickness directly affect the air-gap magnetic field, back EMF, and electromagnetic torque. The motor adopts a multi-pole multi-slot stator structure and a U-shaped interior PM rotor structure, in which magnetic bridges, flux barriers, and local saturation regions exist inside the rotor, making the leakage flux distribution and the magnetic potential difference of the external magnetic circuit relatively complex. The leakage coefficient and reluctivity in the conventional empirical formula cannot accurately reflect such magnetic circuit characteristics, while the FE parametric sweep method requires repeated modeling and calculation for multiple thickness schemes. Therefore, selecting this motor as a case study can effectively validate the capability of the proposed method to rapidly calculate the PM thickness under a complex magnetic circuit structure. The main structural parameters of this motor are shown in Table 1, and the FE model is shown in Fig. 2.

Table 1. Partial Parameters of the Motor

Name	Result
Rated power(kW)	1600
Rated voltage (kV)	3.6
Rated speed (r/min)	250
Rated torque (kN·m)	61.1
Number of slots	90
Number of pole pairs	10
Outer diameter of stator(mm)	1180
Inner diameter of rotor(mm)	865
Core length(mm)	750

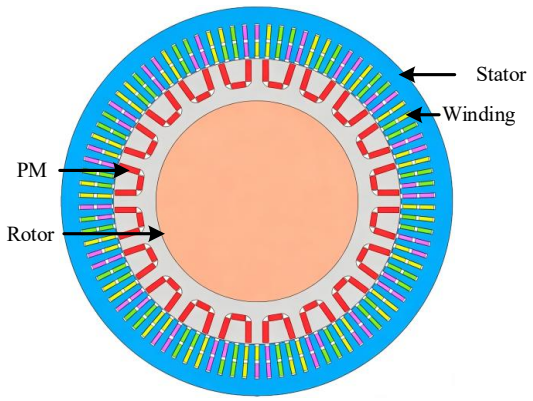


Fig. 2. Finite-Element Model of the Motor

To reduce the complexity of FE modeling, the following assumptions are made in the two-dimensional transient electromagnetic field analysis in this paper:

1.End effects are neglected, the magnetic field is assumed to be uniformly distributed along the axial direction, and the current density vector and magnetic vector potential vector have only the z-direction component.

2.The stator and rotor core materials and the PM material are all regarded as isotropic materials; the nonlinear magnetization characteristics of the core material are described by the B-H curve, and the influence of temperature on material parameters is neglected.

3. The influence of displacement current is ignored, and the electromagnetic field of the motor is considered to satisfy the quasi-static field assumption.

Based on the above assumptions, a two-dimensional transient electromagnetic field model is established using the magnetic vector potential method in this paper, and its governing equation is [15]:

$$\frac{\partial}{\partial x}(\nu\frac{\partial A_z}{\partial x})+\frac{\partial}{\partial y}(\nu\frac{\partial A_z}{\partial y})=-J_z+\sigma_c\frac{\partial A_z}{\partial t} \tag{24}$$

where A_z is the magnetic vector potential in the z-direction, ν is the magnetic reluctivity, J_z is the current density in the z-direction, σ_c is the electrical conductivity, and t is the time. By solving this model, the no-load air-gap flux density, total PM flux, main air-gap flux, and magnetic potential drops in various parts can be obtained, providing a data basis for the subsequent iterative calculation of the PM thickness [16].

3.2 Calculated Results of PM Thickness

Based on the PM material parameters and motor structural dimensions, initial parameters such as the remanence, relative recoil permeability, pole-arc coefficient, and air-gap length of the PM are determined. The initial PM thickness $h_m^{(0)}$ is obtained through estimation, and the corresponding FE model is established. Under the no-load condition, the total PM flux, main air-gap flux, and magnetic potential difference in various parts are extracted, and the leakage coefficient, reluctivity, and average air-gap flux density are calculated. The no-load flux distribution at the initial thickness is shown in Fig. 3. The above parameters are substituted into the thickness calculation formula proposed in this paper to obtain the next PM thickness $h_m^{(i+1)}$, and the iteration is repeated until the convergence condition is satisfied. The calculation results under different iteration numbers are shown in Table 2.

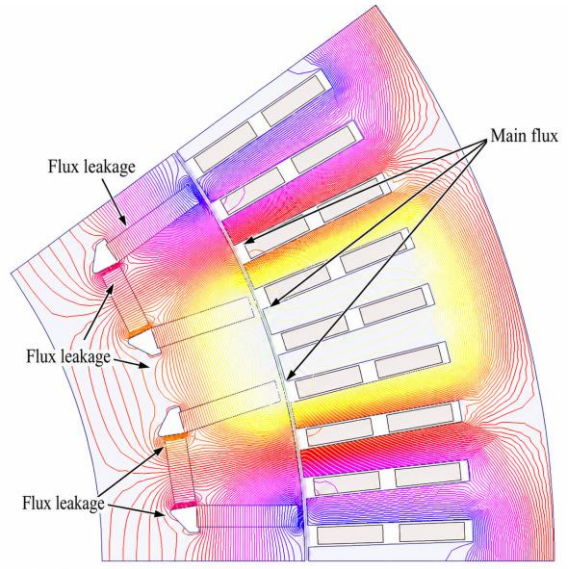


Fig. 3. No-load magnetic flux distribution under the initial PM thickness.

As shown in Fig. 3, the magnetic flux lines mainly originate from the rotor PMs, pass through the air gap into the stator teeth, and close along the stator yoke, forming the main magnetic flux path, which is mainly concentrated in the air-gap region corresponding to the PMs and near the stator teeth. Meanwhile, the figure shows locally closed magnetic flux lines at the ends of the PMs, near the rotor magnetic bridges, flux barriers, and between adjacent PMs, indicating that a portion of the flux does not enter the main air-gap circuit but forms leakage flux within the rotor. This leakage phenomenon reduces the utilization rate of the PM flux; therefore, it is necessary to introduce a leakage coefficient in the thickness calculation and update it through FE post-processing[17].

Table 2. Iterative calculation results of PM thickness.

Name	1	2	3	4	5	6	7
h_m	13.39	14.20	14.97	15.72	16.33	16.80	17.06
σ	1.239	1.223	1.207	1.194	1.182	1.173	1.186
K_R	1.279	1.300	1.317	1.340	1.360	1.376	1.404
μ_r	1.08	1.08	1.08	1.08	1.08	1.08	1.08
α_p	0.75	0.75	0.75	0.75	0.75	0.75	0.75
δ_e	2.5	2.5	2.5	2.5	2.5	2.5	2.5
B_{avg}	0.644	0.656	0.666	0.675	0.683	0.689	0.682
B_r	1.23	1.23	1.23	1.23	1.23	1.23	1.23
ε	5.75	5.70	5.14	4.77	3.74	2.80	1.52

As can be seen from Table 2, with the increase in the number of iterations, the leakage coefficient gradually changed from 1.239 to 1.186, the reluctance coefficient increased from 1.279 to 1.404, the average flux density fluctuated slightly within the range of 0.644-0.689 T and finally stabilized at about 0.682 T, and the PM thickness increased from the initial 13.39 mm to 17.06 mm, with the magnitude of thickness change gradually decreasing. The relative error between two consecutive iterations decreased from 5.75% to 1.52%, satisfying the convergence criterion of 2% set in this paper. The proposed method can continuously correct the leakage coefficient, reluctivity, and average flux density through the FE post-processing results, enabling the PM thickness to converge step by step [18-19]. The final calculated thickness is 17.06 mm, and it is taken as 17.00 mm after considering the actual machining accuracy. To further verify the rationality of the calculation method proposed in this paper, a comparative analysis is conducted among the FE parametric sweep method, the traditional empirical formula method, and the proposed calculation method. The calculation results of the three methods are shown in Table 3.

Table 3. Comparison of thickness results among different calculation methods.

Name	FE Parametric Sweep	Traditional formulas	Paper's method
Time(s)	1200	10	300
Thickness(mm)	17.00	17.82	17.00

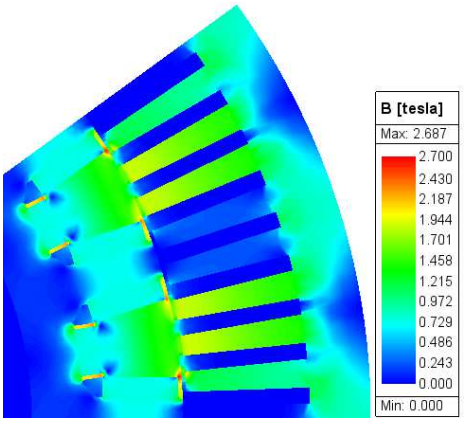
As can be seen from Table 3, the PM thickness obtained by the FE parametric sweep method is 17.00 mm, and because repeated modeling and solving are required for multiple thickness schemes, the calculation time reaches 1200 s. The traditional empirical formula method takes only 10 s to calculate, and the calculated thickness is 17.82 mm, which is larger than the FE parametric sweep result. The proposed method yields a calculated PM thickness of 17.06 mm, which is taken as 17.00 mm after considering the actual machining accuracy, consistent with the result of the FE parametric sweep method; in contrast, the calculation time of the proposed method is 300 s, which is 75% shorter than that of the FE parametric sweep. Since the final adopted values of both the FE parametric sweep method and the proposed method are 17.00 mm, they are treated as the same thickness scheme in the subsequent electromagnetic performance analysis, and will be compared with the 17.82 mm scheme obtained by the traditional empirical formula method.

4 Comparative analysis of electromagnetic performance for different calculation schemes.

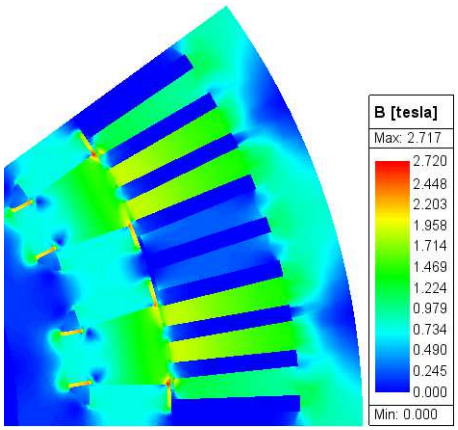
4.1 No-Load Electromagnetic Performance

Comparison

No-load electromagnetic performance serves as an important basis for evaluating the rationality of the PM thickness. To verify the effectiveness of the 17.00 mm thickness scheme obtained by the proposed method, it is compared with the 17.82 mm scheme derived from the traditional empirical formula method, and the flux density distribution, air-gap flux density waveform, and no-load back-EMF waveform are extracted under the same no-load operating condition. The no-load flux density distributions for the two thickness schemes are shown in Fig. 4, and the air-gap flux density waveform and no-load back-EMF waveform are shown in Fig. 5.



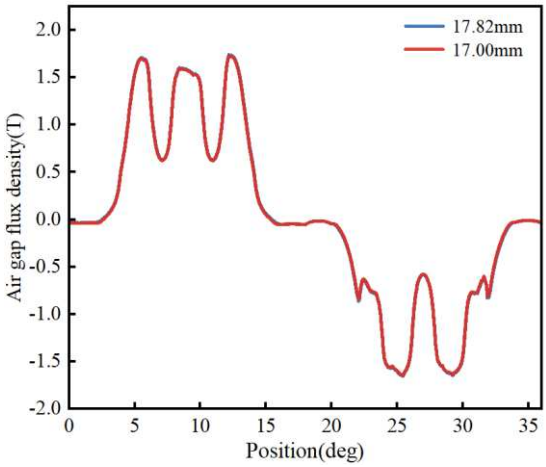
(a). 17.00mm



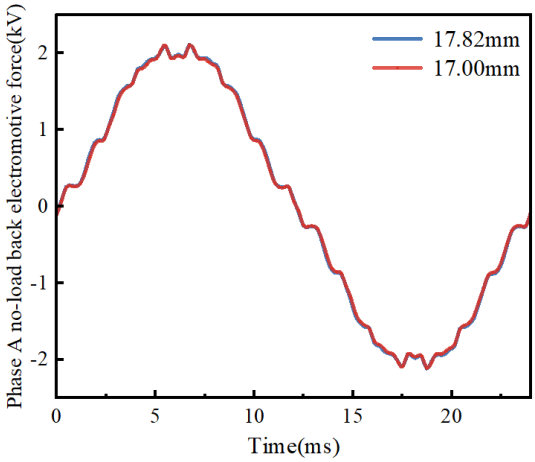
(b). 17.82mm

Fig. 4. No-load flux density distributions under different thickness schemes.

As shown in Fig. 4, comparing Fig. 4(a) and Fig. 4(b), when the PM thickness increases from 17.00 mm to 17.82 mm, the maximum flux density rises from 2.687 T to 2.717 T, an increase of merely 0.03 T. This indicates that increasing the PM thickness has little influence on the overall flux density distribution and does not significantly enhance the main air-gap magnetic field. Meanwhile, the 17.82 mm scheme exhibits a slightly higher local maximum flux density, indicating that a larger thickness aggravates the local saturation near the stator tooth tips and rotor magnetic bridges. In contrast, the 17.00 mm scheme maintains an effective main magnetic circuit while exhibiting a lower local flux density level. Therefore, the 17.00 mm thickness scheme obtained by the proposed method possesses better rationality [20].



(a). Air-gap flux density waveform



(b). No-load back-EMF waveform

As can be seen from Fig. 5, in Fig. 5(a), the amplitudes and waveform trends of the air-gap flux density for the two schemes are basically consistent, indicating that the 17.00 mm scheme can already establish an effective main air-gap magnetic field. In Fig. 5(b), the no-load back-EMF waveforms and peak values of the two schemes are also relatively close, indicating that further increasing the PM thickness has a limited effect on improving the PM flux linkage and induced electromotive force. Therefore, the 17.00 mm thickness scheme obtained by the proposed method has already met the no-load performance requirements, while the 17.82 mm scheme obtained by the traditional empirical formula does not bring significant performance improvement.

4.2 Load Electromagnetic Performance Comparison

The on-load electromagnetic performance serves as an important basis for evaluating whether the PM thickness scheme meets the output requirements. To verify the load performance of the 17.00 mm scheme obtained by the proposed method, FE calculations are performed on both the 17.00 mm and 17.82 mm schemes under rated

conditions, and their electromagnetic torque waveforms, average torque, and torque ripple are compared. The load torque waveforms under the two thickness schemes are shown in Fig. 6.

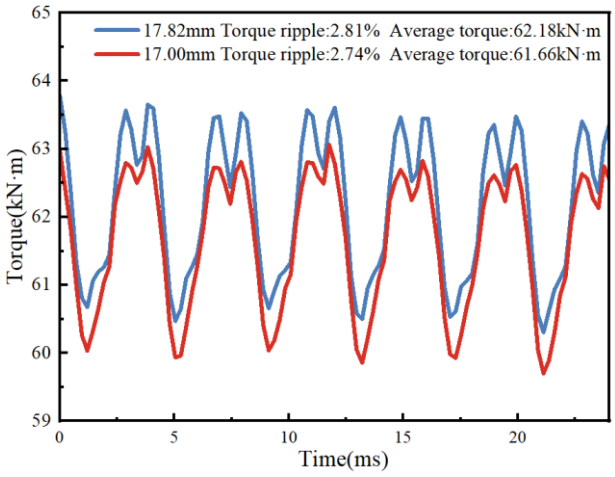


Fig. 6. Analysis of torque characteristics under different thickness schemes.

As shown in Fig. 6, at the same current, the torque waveform trends are nearly identical for the two thickness designs; the 17.82 mm design yields an average torque of 62.18 kN·m, while the 17.00 mm design produces 61.66 kN·m. Compared with the 17.00 mm scheme, the average torque of the 17.82 mm scheme is increased by only about 0.84%, representing a marginal improvement. Meanwhile, the torque ripple of the 17.82 mm scheme is 2.81%, which is slightly higher than the 2.74% of the 17.00 mm scheme. Therefore, under the same current, increasing the PM thickness yields limited improvement in average torque and does not reduce torque ripple. The 17.00 mm scheme can meet the rated torque output requirement and has lower torque ripple, indicating that this thickness scheme possesses better rationality.

4.3 Comprehensive Performance Comparison of the Motor

To further evaluate the comprehensive performance of different PM thickness schemes, this paper compares three aspects: PM utilization, losses, and efficiency. Since the number of PMs, magnet width, and core length remain the same for both schemes, the PM volume is primarily determined by the thickness. Therefore, λ_{PM} is adopted as the evaluation indicator for PM material utilization, and its expression is [21]:

$$\lambda_{PM} = \frac{T_{\text{avg}}}{V_{PM}} \tag{25}$$

Therefore, the comprehensive performance comparison of the motor under different thickness schemes obtained through FE calculation is shown in Table 4.

Table 4. Comprehensive performance comparison of the motor under different thickness schemes.

Name	17.00mm	17.82mm
PM loss (kW)	38.9	40.7
Iron loss (kW)	88.4	89.1
Copper loss (kW)	23.6	23.6
Efficiency (%)	91.38	91.25
PM utilization factor ((N·m)/cm^3)	14.39	13.84

As shown in Table 4, under the same current condition, the copper losses of the two schemes remain identical at 23.6 kW. Compared with the 17.00 mm scheme, the increased magnetic loading of the 17.82 mm scheme causes the iron loss to rise slightly from 88.4 kW to 89.1 kW, while the PM eddy-current loss increases from 38.9 kW to 40.7 kW. Consequently, the efficiency decreases from 91.38% to 91.25%. In addition, the PM utilization factor decreases from 14.39 to 13.84 N·m/cm^3, indicating that the torque improvement is lower than the increase in PM volume. Therefore, the 17.00 mm scheme provides lower losses, higher efficiency, and better PM utilization.

5 Experimental Verification

To verify the accuracy of the FE model and support the electromagnetic performance analysis results presented earlier, a prototype of a 1600 kW, 20-pole 90-slot U-shaped interior PMSM was manufactured according to the 17.00 mm PM thickness scheme in this paper. The geometric dimensions, winding parameters, PM material, and core material of the prototype were kept consistent with the FE model to ensure the comparability between the experimental and simulation results. Fig. 7 shows the physical structures of the stator laminations and rotor assembly of the prototype, and Fig. 8 presents the test platform and main test equipment. This chapter verifies the accuracy of the finite element model in predicting the electromagnetic performance of the motor by comparing the experimental and simulation results of the rated torque and peak torque, and further demonstrates the engineering feasibility of the 17.00 mm PM thickness scheme obtained in this paper.



(a) Rotor structure. (b) Stator structure.
Fig. 7. Motor structure

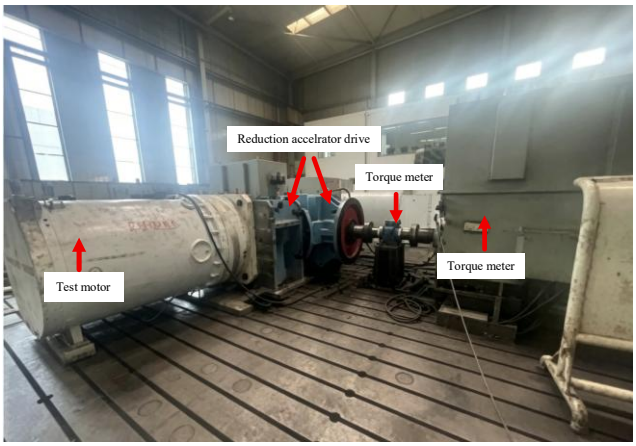


Fig. 8. Test platform

The experiment was carried out in accordance with the load test method specified in IEC 60034-2-3:2024 standard [21]. The main test equipment included a 30 kN·m torque-speed sensor, a broadband current clamp meter, a digital thermometer, a DC low-resistance tester, and a high-power variable-frequency drive system, which were used to measure parameters such as the torque, speed, current, voltage, and temperature rise of the motor under various operating conditions. As shown in Fig. 8, the test platform adopted a variable-frequency drive system to drive the 1600 kW prototype, and used a 2000 kW three-phase asynchronous motor as the load, which was connected to the tested motor through a two-stage gearbox. The rated speed of the tested prototype was 250 r/min, and the rated torque was 61.1 kN·m; after conversion through the two-stage gearbox, the load-side speed was 1250 r/min, corresponding to a torque of 12.25 kN·m. The test platform was equipped with an asynchronous load motor with a rated torque of 12.7 kN·m and a 30 kN·m torque meter, which could meet the rated and peak torque testing requirements of the prototype. According to the test requirements, the rated torque of the motor under test was 61.1 kN·m, and the peak torque was required to be no less than 150% of the rated torque. Table 5 presents the comparison results between the experimental torque values and the finite element simulation values of the prototype. As can be seen from Table 5, the simulation errors for the rated torque and peak torque are 0.90% and 0.76%, respectively, both of which are within the permissible engineering range. The experimental results agree well with the simulation results, indicating that the established finite element model can accurately predict the torque performance of the motor, and also providing a reliable basis for the simulation comparison and analysis of different PM thickness schemes presented earlier.

Table 6. Comparison between measured and simulated torque

Name	T_n	T_{max}
Test (kN·m)	61.10	91.70
Simulation (kN·m)	61.66	92.40
Error (%)	0.90	0.76

6 Conclusion

This paper proposes an iterative PM-thickness calculation method and validates it on a 1600-kW, 250-r/min interior PMSM. By updating the leakage coefficient, reluctivity, and average air-gap flux density through FE post-processing, the proposed method obtains the same final PM thickness as the FE parametric sweep while reducing the computation time by approximately 75%. Moreover, the resulting 17.00-mm scheme maintains comparable no-load and load performance to the 17.82-mm scheme, while achieving lower iron and PM eddy-current losses, higher efficiency, and better PM utilization, thereby demonstrating improved computational efficiency and overall design rationality.

Funding

This work was supported by the National Natural Science Foundation of China project under grant no 62473061 and General Project of Liaoning Provincial Department of Education under grant no LJ212410167024 and Doctoral Research Startup Project of Liaoning Provincial Department of Science and Technology under grant no 2025BS0809

Data availability

Authors declare no competing interests.

Conflict of interest Authors are declaring there is no conflict of interest to report in this study.

References

1. Diyar H, Eker M, Akar M. Electromagnetic design and experimental validation of a low-power IPM motor[J]. Electrical Engineering, 2026, 108(5): 269.
2. Zharkov E, Shayhlislamov A, Okhotnikov M. Stator winding design for a high specific power aircraft propulsion motor[J]. Electrical Engineering, 2026, 108(2): 123.
3. Vatani M, Mohammadi A, Lewis D D, et al. Axial flux permanent magnet generators for direct-drive wind turbines-review and optimal design studies[J]. IEEE Transactions on Industry Applications, 2025, 61(6): 9615-9627.
4. Park J H, Hong D K. Design and comprehensive analysis of magnetic-geared permanent magnet synchronous motor for single-propeller underwater propulsion[J]. IEEE Access, 2025.
5. Mi C, Filippa M, Liu W, et al. Analytical method for predicting the air-gap flux of interior-type permanent-magnet machines[J]. IEEE Transactions on Magnetics, 2004, 40(1): 50-58.
6. Le A T, Lan N T, Do N Y, et al. Studying the effect of PM thickness on the back-EMF and power factor of LSPMSM[J]. Journal Européen des Systèmes Automatisés, 2025, 58(3): 493.
7. Wu S, Wang B, Zhang T, et al. Design optimization and electromagnetic performance analysis of an axial-flux permanent magnet brushless DC motor with unequal-thickness magnets[J]. Applied Sciences, 2022, 12(15): 7863.
8. Chen H, Lee C H T. Parametric sensitivity analysis and design optimization of an interior permanent magnet

synchronous motor[J]. IEEE Access, 2019, 7: 159918-159929.
9. Cabuk A S. Simulation of the effect of segmented axial direction magnets on the efficiency of in-wheel permanent magnet brushless DC motors used in light electric vehicles based on finite element method[J]. Electrical Engineering, 2021, 103(6): 3111-3117.
10. Yazdan T, Humza M, Ali Q, et al. Design and analysis of a two-phase brushless DC motor with hybrid permanent magnet material for only-pull drive technique[J]. Electrical Engineering, 2021, 103(5): 2335-2343.
11. Paiva Jr R D, Silva V C, Nabeta S I, et al. Magnetic topology with axial flux concentration: a technique to improve permanent-magnet motor performance[J]. Journal of Microwaves, Optoelectronics and Electromagnetic Applications, 2017, 16(4): 881-899.
12. Li M, Wang R, Chi L, et al. Analysis of the Influence of Time Harmonics on the Leakage Coefficient of Canned Permanent Magnet Synchronous Motors[J]. Electronics, 2024, 13(23): 4846.
13. Kim S, Jung W S, Kim W H, et al. Optimal design of permanent magnet synchronous machine based on random walk method and semi 3D magnetic equivalent circuit considering overhang effect[J]. Energies, 2022, 15(21): 7852.
14. Feng Y, Zhang C. Analytical calculation for predicting the air gap flux density in surface-mounted permanent magnet synchronous machine[J]. Journal of Electrical Engineering and Technology, 2017, 12(2): 769-777.
15. Ion I G, Bontinck Z, Loukrezis D, et al. Robust shape optimization of electric devices based on deterministic optimization methods and finite-element analysis with affine parametrization and design elements[J]. Electrical Engineering, 2018, 100(4): 2635-2647.
16. Darmani M A, Cavagnino A, Vaschetto S, et al. Multiphysics Sizing of Interior Permanent Magnet Machines Based on Geometric Methodology[J]. IEEE Open Journal of Industry Applications, 2024, 5: 283-299.
17. Sizov G Y, Ionel D M, Demerdash N A O. Modeling and design optimization of PM AC machines using computationally efficient-finite element analysis[C]//2010 IEEE Energy Conversion Congress and Exposition. IEEE, 2010: 578-585.
18. Yeo H K, Lim D K, Jung H K. Magnetic equivalent circuit model considering the overhang structure of an interior permanent-magnet machine[J]. IEEE Transactions on Magnetics, 2019, 55(6): 1-4.
19. Yeo H K, Lim D K, Jung H K. Magnetic equivalent circuit model considering the overhang structure of an interior permanent-magnet machine[J]. IEEE Transactions on Magnetics, 2019, 55(6): 1-4.
20. Wang M, Zhu H, Zhou C, et al. Analysis and optimization of a V-shape combined pole interior permanent-magnet synchronous machine with temperature rise and demagnetization considered[J]. IEEE Access, 2021, 9: 64761-64775.
21. Rotating Electrical Machines—Part 2-3: Specific Test Methods for Determining Losses and Efficiency of Converter-Fed AC Motors, IEC Standard 60034-2-3, 2nd ed., Mar. 2024.